Chern numbers and chiral anomalies in Weyl butterflies

Sthitadhi Roy, Michael Kolodrubetz, Joel E. Moore, and Adolfo G. Grushin

Phys. Rev. B **94**, 161107 — Published 6 October 2016

DOI: 10.1103/PhysRevB.94.161107

Chern numbers and chiral anomalies in Weyl butterflies

Sthitadhi Roy,[1] Michael Kolodrubetz,[2,3] Joel E. Moore,[2,3] and Adolfo G. Grushin[3]

[1] *Max-Planck-Institut für Physik komplexer Systeme, Nöthnitzer Straße 38, 01187 Dresden, Germany*
[2] *Materials Sciences Division, Lawrence Berkeley National Laboratory, Berkeley, CA 94720, USA*
[3] *Department of Physics, University of California, Berkeley, CA 94720, USA*

The Hofstadter butterfly of lattice electrons in a strong magnetic field is a cornerstone of condensed matter physics, exploring the competition between periodicities imposed by the lattice and the field. In this work we introduce and characterize the Weyl butterfly, which emerges when a large magnetic field is applied to a three-dimensional Weyl semimetal. Using an experimentally motivated lattice model for cold atomic systems, we solve this problem numerically. We find that Weyl nodes reemerge at commensurate fluxes and propose using wavepackets dynamics to reveal their chirality and location. Moreover, we show that the chiral anomaly – a hallmark of the topological Weyl semimetal – does not remain proportional to magnetic field at large fields, but rather inherits a fractal structure of linear regimes as a function of external field. The slope of each linear regime is determined by the difference of two Chern numbers in gaps of the Weyl butterfly and can be measured experimentally in time-of-flight.

Introduction – The search for novel phenomena in condensed matter is often spurred by competing physical effects acting on comparable length scales. A central example is the response of fermions on a lattice to an external magnetic field when the magnetic length l_B becomes comparable to the lattice spacing a. The energy spectrum displays a fractal structure known as the Hofstadter butterfly [1], that is invariant upon changing applied field by one magnetic flux quantum $\Phi_0 = h/e$ per unit cell. Furthermore, the gaps that separate sub-bands are characterized by a two-dimensional topological Chern number.

Topological invariants generally yield non-trivial condensed matter phenomena, as in topological insulators [2, 3] and more recently Weyl and Dirac semimetals [4–6]. These semimetals host pairs of protected band touchings (nodes) that disperse linearly with momentum. Each pair is composed of a left and right chirality node, a quantum number resembling the valley degree of freedom in graphene. Although the sum of right- and left-handed fermions is conserved, non-orthogonal magnetic ($\mathbf{B}$) and electric ($\mathbf{E}$) fields pump one chirality to the other at a rate $\propto \mathbf{E}\cdot\mathbf{B}$, so that their difference is not conserved. This phenomenon, known as the chiral anomaly [7, 8], distinguishes conventional metals from topological ones; while the former display positive longitudinal magnetoresistance, the chiral anomaly manifests as negative magnetoresistance in the latter [9, 10], consistent with recent measurements [11–38].

The response of Weyl fermions to external electromagnetic fields is well understood both in the linear response regime [39–46] and the Landau level limit [8, 45, 47–49]. In this work, we uncover a richer structure that emerges for Weyl fermions on a lattice in the Hofstadter regime ($l_B \sim a$), determining the fate of the chiral anomaly in this limit. The non-renormalization theorem of the chiral anomaly beyond one-loop [7] breaks down, and the $\mathbf{B}$-dependence of the anomaly is periodic in units of Φ_0 per unit cell. We find that the chiral anomaly tracked through the rate of chiral charge pumping shows a fractal of linear regimes proportional to $\mathbf{B}$ with quantized integer slopes, intimately connected to a fractal set of emergent Weyl nodes at commensurate fluxes. The integer slopes are given by the Chern numbers of the Weyl butterfly – a three-dimensional fractal which describes the spectrum of a Weyl semimetal under large magnetic fluxes. The physics resulting from the third dimension is not a mere generalization of the two-dimensional Hofstadter case. Crucially, we show that there is an analytical connection between the evolution of the fractal

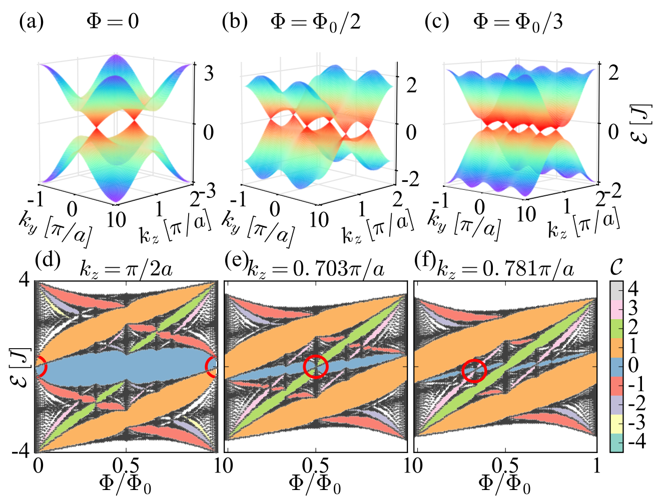

FIG. 1. Energy spectra of Weyl fermions in a magnetic field, as obtained from Eq. (2). **(a)-(c)** New Weyl nodes emerge at commensurate fluxes per plaquette with an additional q-fold degeneracy (see text). **(d)-(f)** Hofstadter-like spectrum for the k_z values where the Weyl nodes appear for the corresponding fluxes shown in (a)-(c). The isolated zeroth Landau level occurring around the Weyl nodes is highlighted by the red circles. The colors in the butterflies denote the Chern number $\mathcal{C}$ in the gap.

spectrum along the third momentum direction, its Chern numbers, and the fractal nature of the chiral anomaly. The work motivated by both fundamental interest [50–57] and plausible experimental realization in cold atomic systems [58–60]. Using a model tightly connected to the experimental proposal in Ref. [58] we show how both the Chern numbers and the chiral anomaly may be directly measured with cold atoms.

Weyl semimetal in magnetic fields – To describe a Weyl semimetal, we employ a two-band Hamiltonian of spinless fermions on a cubic lattice $\mathcal{H}_{\mathbf{k}} = \mathbf{d}_{\mathbf{k}} \cdot \boldsymbol{\sigma}$, with

$$\mathbf{d}_{\mathbf{k}} = -\{J_2 \sin k_x, J_2 \sin k_y, -M + J_1 \sum_{i=x,y,z} \cos k_i\}. \quad (1)$$

This model breaks time-reversal symmetry and is motivated by that in Ref. [58], which is composed of the two time reversal partners of Eq. (1) separated in momentum space. It has a pair of linearly dispersing Weyl cones at $\mathbf{k} = \{0, 0, \pm\cos^{-1}(M/J_1 - 2)\}$ for $1 < |M/J_1| < 3$. We use $J_2 = J_1 = J$ and $M/J = 2$ for the remainder of this paper. Fig. 1(a) shows the band structure in the (k_y, k_z) plane. This model is constructed from Chern insulators in the (k_x, k_y) plane with a k_z dependent gap such that the Chern number $\mathcal{C}_{k_z}$ changes whenever a Weyl node is crossed, as shown by the dashed line in Fig. 2b.

We now consider applying magnetic field $\mathbf{B} \parallel \hat{z}$ with flux $\Phi = \Phi_0 p/q$ per plaquette, equivalent to an Aharonov-Bohm phase of $\phi = 2\pi p/q$ upon tunneling around a plaquette. In the Landau gauge, $\mathbf{A} = \Phi x \hat{y}$, the Hamiltonian becomes

$$\mathcal{H}_{\mathcal{WH}} = \begin{pmatrix} \mathcal{M}_1 & \mathcal{R}/2 & 0 & \cdots & \mathcal{S}/2 \\ \mathcal{R}^\dagger/2 & \mathcal{M}_2 & \mathcal{R}/2 & \cdots & 0 \\ \vdots & \ddots & \ddots & \ddots & \vdots \\ \mathcal{S}^\dagger/2 & 0 & \cdots & \mathcal{R}^\dagger/2 & \mathcal{M}_q \end{pmatrix},$$

$$\begin{aligned} \mathcal{M}_n(k_y, k_z) = \; & [M - J(\cos(k_y + \phi n) + \cos k_z)]\sigma^z - \\ & J \sin(k_y + \phi n)\sigma^y, \end{aligned}$$

$$\mathcal{R} = -J(\sigma^z - i\sigma^x); \; \mathcal{S}(k_x) = -J(\sigma^z + i\sigma^x)e^{-ik_x}. \quad (2)$$

Each k_z exhibits a Hofstadter-like spectrum [61], (see Fig. 1) forming the energy spectrum that we refer to as the Weyl butterfly.

One unexpected aspect of the Weyl butterfly is that, for commensurate fluxes, new pairs of Weyl nodes emerge with q-fold degeneracy unlike the two-dimensional Hofstadter butterfly which has Dirac nodes only for even q. [62] [63, 64] In Fig. 1(d)-(f) we highlight some of the emergent Weyl nodes that cross near $\mathcal{E} = 0$ for particular values of k_z. The emergence of such new Weyl nodes is related to the fractal structure of the butterfly, while the q-fold degeneracy comes from noting that the shift $k_y \to k_y + 2\pi p/q$ in Eq. (2) amounts to changing $\mathbf{A}$ in steps of Φ, which has no effect on the spectrum. Since q such translations traverse the BZ, there should be q copies of the spectrum. [65] Perturbing the flux around one of these emergent Weyl nodes splits it into Landau levels dispersing along k_z, including a chiral zeroth Landau level [8]. As the flux is further increased, the Landau levels split and merge with those of the upcoming Weyl node, a feature which we explore in more detail later.

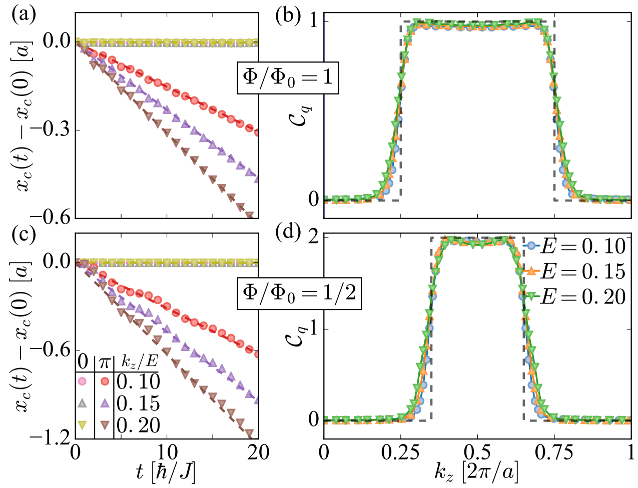

FIG. 2. Hall drift of the center-of-mass of a wavepacket for different values of the electric field E at two representative k_z values, 0 and π, along with the linear fits used to calculate $\mathcal{C}_q$ for $q = 1$ **(a)** and $q = 2$ **(c)**. **(b)** and **(d)** show the topological transition of $\mathcal{C}_q$ at the positions of the Weyl nodes, as obtained from Eq. (4). For the simulations $L = 128$ and $L_s = 48$.

Chern numbers via wavepacket dynamics – A nontrivial topological invariant that characterizes the emergent Weyl nodes at rational flux is the Chern number in each momentum plane. An experimentally feasible probe of this invariant in cold-atomic systems is the semi-classical motion of wavepackets [66, 67], which has successfully been used in both the two-dimensional Hofstadter [68] and Haldane [69] models. The principle is that, under an external force, wavepackets Hall drift transverse to the direction of the force with amplitude proportional to the Chern number.

Here we explore the use of such Hall-like response to characterize the Weyl butterfly. First, we consider preparing a wavepacket sharply peaked around a finite momentum k_z along the axis of Weyl node separation. Such a wavepacket could be achieved experimentally by initially decreasing the lattice depth along the z-direction to create a sharp k_z peak then taking it to the desired k_z via a ramped magnetic field [70] or optical gradient [68], lattice acceleration [71], or Bragg pulse.[72] We then consider a wavepacket initially confined within a $L_s \times L_s$ sub-region of an $L \times L$ lattice ($L_s < L$) in the (x, y) plane [66]. At $t = 0$, the xy-confinement is removed to give approximately uniformly-filled bands in (k_x, k_y) [73] and a constant force $\mathbf{F} = EJ/a\ \hat{y}$ is applied [68, 70, 71] The center-of-mass motion in the n^{th}-band is governed by the semiclassical equations of motion [74]

$$\dot{\mathbf{r}}_c = \boldsymbol{\nabla}_{\mathbf{k}}\mathcal{E}_{n,\mathbf{k}} - \dot{\mathbf{k}} \times \boldsymbol{\Omega}_{n,\mathbf{k}}; \qquad \dot{\mathbf{k}} = \mathbf{F}; \tag{3}$$

where $\mathcal{E}_{n,\mathbf{k}}$ and $\boldsymbol{\Omega}_{n,\mathbf{k}}$ are respectively the energy dispersion and Berry curvature of the band. The net drift of the many-fermion wavepacket can be obtained by integrating Eq. (3) over time and summing over the responses for all the filled bands. For m uniformly filled bands, the drift is [66]

$$\mathbf{r}_c(t) - \mathbf{r}_c(0) = -\frac{Et}{2\pi}\sum_{n=1}^{m} \mathcal{C}_n\ \hat{x} \equiv -\frac{Et}{2\pi}\mathcal{C}_m\ \hat{x}, \tag{4}$$

where $\mathcal{C}_n = (1/2\pi)\int dk_x dk_y\ \Omega^z_{n,\mathbf{k}}$ is the Chern number of the n-th band.

For flux Φ, we can use this technique to measure the sum of the Chern numbers of the q lowest bands, $\mathcal{C}_q$, for emergent Weyl nodes which connect the q^{th} and $(q+1)^{\text{th}}$ bands. The Hall drift given by Eq. (4), and its corresponding C_q are shown in Fig. 2 for two different fluxes as a function of k_z. As k_z crosses a Weyl node, the q^{th} and $(q+1)^{\text{th}}$ bands undergo a topological phase transition where the sign of the gap of the Chern insulator flips. Consequently, since there are q such Weyl points, the Chern number changes by $\pm q$ with sign determined by the chirality of the Weyl nodes. Thus from the wavepacket dynamics as a function of k_z, one can extract the location, chiralities, and multiplicities of the Weyl points.

In experiments, it is often easier to prepare a finite-width distribution of the occupations W_{k_z} than a sharply-peaked k_z. Controlling the width of this distribution through external trapping or temperature also allows to infer information about the spectrum. In this case, the Hall drift with the Fermi level in the q^{th} gap yields a non-quantized effective Chern number, $\mathcal{C}_{q,\text{eff}} = \sum_{k_z}\mathcal{C}_{q,k_z}W_{k_z}$, which is the average of $\mathcal{C}_{q,k_z}$ weighted by W_{k_z}. For instance, if we create Gaussian distributions centered at $k_z = 0$ with width σ for the particular case of two Weyl nodes at $\pm K_0/2$, we find that the dependence of the Hall drift on σ saturates to $\mathcal{C}_{q,\text{eff}} = \mathcal{C}_{q,k_z=\pi/a} - (\mathcal{C}_{q,k_z=\pi/a} - \mathcal{C}_{q,k_z=0})K_0/2\pi$ in the $\sigma \to \infty$ limit and to $\mathcal{C}_{q,\text{eff}} = \mathcal{C}_{q,k_z=0}$ for $\sigma \to 0$. Varying σ interpolates between these limits; a simple fit can then extract the Chern number profile. A more in-depth analysis can be found in the Supplementary material [75].

Chiral anomalies in the Weyl butterfly – We now turn to the main result of our work; the fate of the chiral anomaly in the Hofstadter regime. Our starting point is Eq. (1) at $\Phi = 0$ with chemical potential chosen to be at the Weyl nodes ($\mathcal{E}_F = 0$). Upon applying a finite flux ($\Phi/\Phi_0 \lesssim 1/4$) the spectrum first breaks into Landau levels (cf. Fig. 3a) that disperse with k_z. Due to the chiral anomaly, if an additional electric field is applied at $t = 0$ satisfying $\mathbf{E} \parallel \hat{z}$, we expect the occupancies to shift along k_z turning left-handed into right-handed fermions

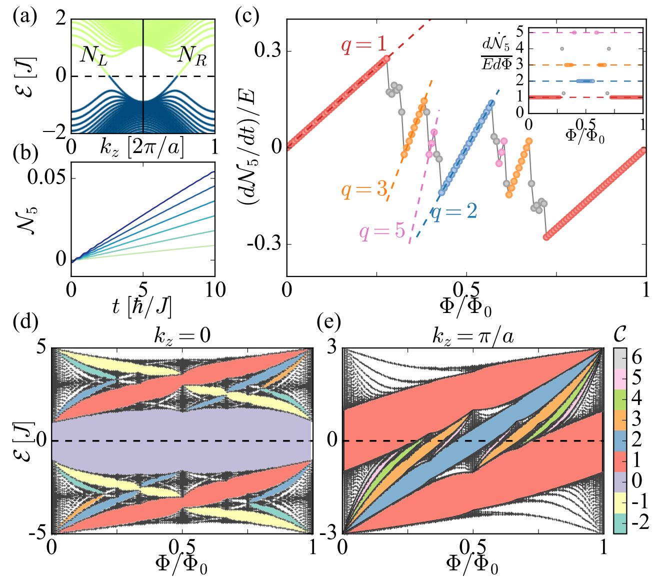

FIG. 3. Chiral anomaly of the Weyl butterfly. **(a)** The chiral charge counts the number difference of left and right movers $\mathcal{N}_5 = (N_L - N_R)/L^2$. **(b)** $\mathcal{N}_5$ increases linearly with time when both E and B are applied as shown for $E = 0.1$ and fluxes $\Phi = n\Phi_0/L$, with n going from 1 to 6 (lighter to darker). **(c)**The rate of chiral charge production grows linearly with the flux with a slope q in the vicinity of commensurate fluxes, for which the model hosts q pairs of Weyl nodes. Linear fits are shown for the data around $\Phi/\Phi_0 = 1, 1/2, 1/3, 2/5$ which correspond to $q = 1, 2, 3, 5$ respectively. Inset: Quantized plateaus corresponding to each linear rate as a function of Φ. The simulations are performed on a cubic lattice with linear dimension L=144. **(d,e)** The magnitude of each plateau can be extracted as described by (7). The slopes in **(c)** are color coded to the Chern numbers in **(d-e)**

via the bottom of the band. To characterize the chiral anomaly we define the chiral charge density

$$\mathcal{N}_5 = \left(\frac{1}{L^2}\right)\sum_{k_y=0}^{2\pi/a}\left[\sum_{k_z=0}^{\pi/a} n_{k_y,k_z} - \sum_{k_z=\pi/a}^{2\pi/a} n_{k_y,k_z}\right], \tag{5}$$

where n_{k_y,k_z} is the total number of filled fermionic states with momentum k_y, k_z. This quantity monitors the amount of charge pumped from one half of the Brillouin zone to another; its rate of increase is proportional to the applied electric field. The definition (5) implies that only the states that cross the Fermi level can contribute to the pumping of chiral charge. For $\Phi/\Phi_0 \lesssim 1/4$ we find that $\mathcal{N}_5$ grows linearly with time (Fig. 3b). In addition, the rate of growth $d\mathcal{N}_5/Edt$ is linear as a function of Φ (Fig. 3c). So far, both of these results are consistent with the conventional chiral anomaly, $d\mathcal{N}_5/dt \propto \mathbf{E}\cdot\mathbf{B}$.

As the flux increased ($\Phi/\Phi_0 > 1/4$) the linear behavior of $d\mathcal{N}_5/Edt$ with Φ breaks down. As shown in Fig. 3c, several linear regimes where $d\mathcal{N}_5/dt \propto \Phi$ appear, with unequal slopes. Each linear regime is centered around commensurate fluxes $\Phi/\Phi_0 = p/q$, with slope quantized

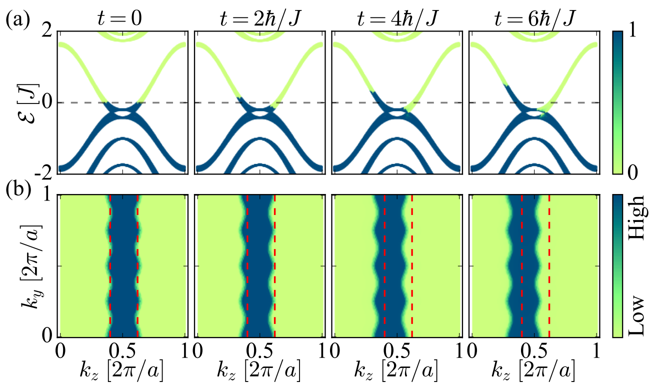

FIG. 4. **(a)** Evolution of occupancies in the bands after an electric field $E = 0.1$ is turned on, showing the development of the chiral anomaly for $\Phi{=}\Phi_0/4$. The dashed horizontal line represents the Fermi level $\mathcal{E}_F$. **(b)** Time-of-flight occupancy profiles in the (k_y, k_z) plane in arbitrary units. The vertical dashed lines serve as a guide to the eye for the initial profile at $t = 0$. Simulation parameters are the same as Fig. 3.

to q. This is a direct consequence of the emergence of q pairs of Weyl nodes, leading to q copies of the Landau levels crossing the Fermi energy. Hence, as the flux is ramped, the Landau level degeneracy grows as $q\Delta\Phi$, leading to chiral charge production $\dot{\mathcal{N}}_5 \propto Eq\Delta\Phi$. The full behaviour is thus composed of jumps between the linear regimes in Fig. 3 around commensurate values of the flux. In the thermodynamic limit the self similar fractal structure of the butterfly implies that these linear regimes should themselves form a fractal of integer valued slopes.

In order to establish a more physical understanding of the fractal nature of the anomaly we now connect it to the Chern number. Recall first that the rate of chiral charge pumping $\dot{\mathcal{N}}_Q/E$ counts the number of chiral channels at the Fermi level. Second, we emphasize that the Weyl butterfly has, for fixed k_z, a series of gaps at $\mathcal{E}_F = 0$ (cf. Fig. 3d-e), each characterized by its Chern number $\mathcal{C}_{k_z}$. The Chern number determines how density is modified when applying a magnetic field through the Streda formula [76]

$$d\rho^{k_z}_{2\mathrm{D}}/dB_z = \mathcal{C}_{k_z}|_{\mathcal{E}_F=0}/\Phi_0 \ . \tag{6}$$

Consider adding one flux quantum to the system $\Phi = \Phi_0/L^2$. For $k_z = 0$, $\mathcal{C} = 0$ at $E_F = 0$, so the density is unaffected. For $k_z = \pi/a$, $\mathcal{C} = 1$, so to increase $\rho_{2\mathrm{D}}$ as in Eq. (6), one conduction level must move to the valence band. The difference must be accommodated in between these momenta, leading to one extra chiral channel. Since, for our inversion-symmetric Weyl semimetal, the Weyl points always appear in $\pm k_z$ pairs with opposite chirality, it suffices to consider $k_z = 0, \pi/a$. This predicts that the chiral anomaly generalizes to

$$(1/E)d\dot{\mathcal{N}}_5/d\Phi = \mathcal{C}_{k_z=\pi/a} - \mathcal{C}_{k_z=0} \ , \tag{7}$$

which is confirmed in Fig. 3c-e. Furthermore, since the butterfly at $k_z = \pi/a$ consists of a fractal set of gapped Chern insulators, we see that the anomaly will become a fractal set of linear anomalies with quantized slopes in the thermodynamic limit. Eq. (7) succinctly summarizes the main findings of this letter. It highlights the topological connection between different k_z sectors which determine the quantized slopes of the chiral anomaly, a result only possible in three-dimensions.

We close by addressing the experimental prospects to probe the chiral anomaly. Lack of reservoirs and relaxation make transport measurements difficult, but this also helps distinguish the chiral anomaly in cold atoms from other competing effects. In practice, the most direct probe is time-of-flight, which directly maps out the momentum-space occupancies. [77] Fig. 4a and Fig. 4b shows the calculated occupancies and time-of-flight images for $\Phi/\Phi_0 = 1/4$ upon applying $\mathbf{E} \parallel \mathbf{B}$ at $t = 0$. The pumping rate $\dot{\mathcal{N}}_5$ can be monitored to probe the chiral anomaly and experimentally access the observables in Fig. 3.

Our analysis extends to models without inversion symmetry, which may have multiple pairs of Weyl nodes. In particular, time-of-flight measurements could track each pair of Weyl nodes independently to measure the chiral pumping. Our results can thus be experimentally tested using existing technology in realistic models such as that in Ref. [58], which already incorporates the high magnetic field necessary for the Weyl butterfly, or the three dimensional variant [78] of the model proposed in Ref. [79]. Finally, we expect these effects to be robust to weak interactions [80, 81] and disorder [47, 82, 83] leaving the effect of strong perturbations for future research.

Conclusion – We have shown that the chiral anomaly generalizes to a quantized fractal in the high-magnetic-field limit, connecting the longitudinal chiral anomaly response to the transverse Hall response characterized by the Chern number. Our results hold for any model of Weyl semimetal with inversion symmetry. The evolution of the spectral butterfly in the third momentum direction determines the universal three-dimensional physics of the chiral anomaly which is summarized by Eq. (7). This particular interplay between two-dimensional planes and the emergence of Weyl nodes for all q distinguishes the Weyl butterfly from two-dimensional [1], and three-dimensional variants of the Hofstadter problem [50–57] and opens the possibility of exploring generic features that relate different models.

Acknowledgements – AGG acknowledges financial support from the European Commission under the Marie Curie Programme. We thank C. Kennedy for useful insights on the experimental feasibility of this proposal. MK and JEM were supported by Laboratory Directed Research and Development (LDRD) funding from Berkeley Lab, provided by the Director, Office of Science, of the U.S. Department of Energy under Contract No.

DEAC02-05CH11231, and JEM acknowledges a Simons Investigator grant.

[1] Douglas R. Hofstadter, "Energy levels and wave functions of bloch electrons in rational and irrational magnetic fields," Phys. Rev. B **14**, 2239–2249 (1976).

[2] M. Z. Hasan and C. L. Kane, "Topological insulators," Rev. Mod. Phys. **82**, 3045 (2010).

[3] Xiao-Liang Qi and Shou-Cheng Zhang, "Topological insulators and superconductors," Rev. Mod. Phys. **83**, 1057–1110 (2011).

[4] Pavan Hosur and Xiaoliang Qi, "Recent developments in transport phenomena in Weyl semimetals," Comptes Rendus Physique **14**, 857–870 (2013).

[5] Ari M Turner and Ashvin Vishwanath, "Beyond Band Insulators: Topology of Semi-metals and Interacting Phases," arXiv:1301.0330.

[6] Oskar Vafek and Ashvin Vishwanath, "Dirac Fermions in Solids: From High-T cCuprates and Graphene to Topological Insulators and Weyl Semimetals," Annu. Rev. Condens. Matter Phys. **5**, 83–112 (2014).

[7] Reinhold A Bertlmann, *Anomalies in quantum field theory*, Vol. 91 (Oxford University Press, 2000).

[8] H.B. Nielsen and Masao Ninomiya, "The Adler-Bell-Jackiw anomaly and Weyl fermions in a crystal," Phys. Lett. B **130**, 389–396 (1983).

[9] D T Son and B Z Spivak, "Chiral anomaly and classical negative magnetoresistance of Weyl metals," Phys. Rev. B **88**, 104412 (2013).

[10] A A Burkov, "Negative longitudinal magnetoresistance in Dirac and Weyl metals," arXiv (2015), 1505.01849.

[11] S-Y Xu, C. Liu, S. K. Kushwaha, T.-R. Chang, J. W. Krizan, R. Sankar, C. M. Polley, J. Adell, T. Balasubramanian, K. Miyamoto, N. Alidoust, G. Bian, M. Neupane, I. Belopolski, H.-T. Jeng, C.-Y. Huang, W.-F. Tsai, H. Lin, F. C. Chou, T. Okuda, A. Bansil, R. J. Cava, and M. Z. Hasan, arXiv:1312.7624.

[12] Heon-Jung Kim, Ki-Seok Kim, J.-F. Wang, M. Sasaki, N. Satoh, A. Ohnishi, M. Kitaura, M. Yang, and L. Li, "Dirac versus weyl fermions in topological insulators: Adler-bell-jackiw anomaly in transport phenomena," Phys. Rev. Lett. **111**, 246603 (2013).

[13] Junya Feng, Yuan Pang, Desheng Wu, Zhijun Wang, Hongming Weng, Jianqi Li, Xi Dai, Zhong Fang, Youguo Shi, and Li Lu, "Large linear magnetoresistance in dirac semimetal cd_3as_2 with fermi surfaces close to the dirac points," Phys. Rev. B **92**, 081306 (2015).

[14] Sergey Borisenko, Quinn Gibson, Danil Evtushinsky, Volodymyr Zabolotnyy, Bernd Büchner, and Robert J. Cava, "Experimental Realization of a Three-Dimensional Dirac Semimetal," Phys. Rev. Lett. **113**, 027603 (2014).

[15] Qiang Li, Dmitri E. Kharzeev, Cheng Zhang, Yuan Huang, I. Pletikosic, A. V. Fedorov, R. D. Zhong, J. A. Schneeloch, G. D. Gu, and T. Valla, arXiv:1412.6543.

[16] Z. K. Liu, B. Zhou, Y. Zhang, Z. J. Wang, H. M. Weng, D. Prabhakaran, S.-K. Mo, Z. X. Shen, Z. Fang, X. Dai, Z. Hussain, and Y. L. Chen, "Discovery of a three-dimensional topological dirac semimetal, na3bi," Science **343**, 864–867 (2014).

[17] Madhab Neupane, Su-Yang Xu, Raman Sankar, Nasser Alidoust, Guang Bian, Chang Liu, Ilya Belopolski, Tay-Rong Chang, Horng-Tay Jeng, Hsin Lin, Arun Bansil, Fangcheng Chou, and M. Zahid Hasan, "Observation of a three-dimensional topological Dirac semimetal phase in high-mobility Cd_3As_2," Nat. Commun. **5** (2014).

[18] Hemian Yi, Zhijun Wang, Chaoyu Chen, Youguo Shi, Ya Feng, Aiji Liang, Zhuojin Xie, Shaolong He, Junfeng He, Yingying Peng, Xu Liu, Yan Liu, Lin Zhao, Guodong Liu, Xiaoli Dong, Jun Zhang, M. Nakatake, M. Arita, K. Shimada, H. Namatame, M. Taniguchi, Zuyan Xu, Chuangtian Chen, Xi Dai, Zhong Fang, and X. J. Zhou, "Evidence of Topological Surface State in Three-Dimensional Dirac Semimetal Cd_3As_2," Sci. Rep. **4** (2014).

[19] Z. K. Liu, J. Jiang, B. Zhou, Z. J. Wang, Y. Zhang, H. M. Weng, D. Prabhakaran, S-K. Mo, H. Peng, P. Dudin, T. Kim, M. Hoesch, Z. Fang, X. Dai, Z. X. Shen, D. L. Feng, Z. Hussain, and Y. L. Chen, "A stable three-dimensional topological Dirac semimetal Cd_3As_2," Nat. Mater. **13**, 677–681 (2014).

[20] L. P. He, X. C. Hong, J. K. Dong, J. Pan, Z. Zhang, J. Zhang, and S. Y. Li, "Quantum Transport Evidence for the Three-Dimensional Dirac Semimetal Phase in Cd_3As_2," Phys. Rev. Lett. **113**, 246402 (2014).

[21] Xiaochun Huang, Lingxiao Zhao, Yujia Long, Peipei Wang, Dong Chen, Zhanhai Yang, Hui Liang, Mianqi Xue, Hongming Weng, Zhong Fang, Xi Dai, and Genfu Chen, "Observation of the Chiral-Anomaly-Induced Negative Magnetoresistance in 3D Weyl Semimetal TaAs," Phys. Rev. X **5**, 031023 (2015).

[22] C. Zhang, S.-Y. Xu, I. Belopolski, Z. Yuan, Z. Lin, B. Tong, N. Alidoust, C.-C. Lee, S.-M. Huang, H. Lin, M. Neupane, D. S. Sanchez, H. Zheng, G. Bian, J. Wang, C. Zhang, T. Neupert, M. Zahid Hasan, and S. Jia, arXiv:1503.02630.

[23] Jun Xiong, Satya K. Kushwaha, Tian Liang, Jason W. Krizan, Max Hirschberger, Wudi Wang, R. J. Cava, and N. P. Ong, "Evidence for the chiral anomaly in the Dirac semimetal Na3Bi," Science **350**, 413–416 (2015).

[24] X. Yang, Y. Li, Z. Wang, Y. Zhen, and Z.-A. Xu, arXiv:1506.02283.

[25] Frank Arnold, Chandra Shekhar, Shu-Chun Wu, Yan Sun, Ricardo Donizeth dos Reis, Nitesh Kumar, Marcel Naumann, Mukkattu O. Ajeesh, Marcus Schmidt, Adolfo G. Grushin, Jens H. Bardarson, Michael Baenitz, Dmitry Sokolov, Horst Borrmann, Michael Nicklas, Claudia Felser, Elena Hassinger, and Binghai Yan, "Negative magnetoresistance without well-defined chirality in the weyl semimetal tap," Nat Commun (2016).

[26] Jianhua Du, Hangdong Wang, Qianhui Mao, Rajwali Khan, Binjie Xu, Yuxing Zhou, Yannan Zhang, Jinhu Yang, Bin Chen, Chunmu Feng, and Fang Minghu, "Unsaturated both large positive and negative magnetoresistance in weyl semimetal tap," arXiv:1507.05246.

[27] Chenglong Zhang, Cheng Guo, Hong Lu, Xiao Zhang, Zhujun Yuan, Ziquan Lin, Junfeng Wang, and Shuang Jia, "Large magnetoresistance over an extended temperature regime in monophosphides of tantalum and niobium," Phys. Rev. B **92**, 041203 (2015).

[28] H. Li, H. He, H.-Z. Lu, H. Zhang, H. Liu, R. Ma, Z. Fan, S.-Q. Shen, and J. Wang, "Negative Magnetoresistance in Dirac Semimetal Cd3As2," Nat. Commun. **7**, 10301 (2016).

[29] Hongming Weng, Chen Fang, Zhong Fang, B. Andrei Bernevig, and Xi Dai, "Weyl semimetal phase in noncentrosymmetric transition-metal monophosphides," Phys. Rev. X **5**, 011029 (2015).
[30] Shin-Ming Huang, Su-Yang Xu, Ilya Belopolski, Chi-Cheng Lee, Guoqing Chang, BaoKai Wang, Nasser Alidoust, Guang Bian, Madhab Neupane, Chenglong Zhang, Shuang Jia, Arun Bansil, Hsin Lin, and M. Zahid Hasan, "A Weyl Fermion semimetal with surface Fermi arcs in the transition metal monopnictide TaAs class," Nat. Commun. **6** (2015).
[31] Su-Yang Xu, Ilya Belopolski, Nasser Alidoust, Madhab Neupane, Guang Bian, Chenglong Zhang, Raman Sankar, Guoqing Chang, Zhujun Yuan, Chi-Cheng Lee, Shin-Ming Huang, Hao Zheng, Jie Ma, Daniel S. Sanchez, BaoKai Wang, Arun Bansil, Fangcheng Chou, Pavel P. Shibayev, Hsin Lin, Shuang Jia, and M. Zahid Hasan, "Discovery of a weyl fermion semimetal and topological fermi arcs," Science **349**, 613–617 (2015).
[32] B. Q. Lv, H. M. Weng, B. B. Fu, X. P. Wang, H. Miao, J. Ma, P. Richard, X. C. Huang, L. X. Zhao, G. F. Chen, Z. Fang, X. Dai, T. Qian, and H. Ding, "Experimental Discovery of Weyl Semimetal TaAs," Phys. Rev. X **5**, 031013 (2015).
[33] Su-Yang Xu, Nasser Alidoust, Ilya Belopolski, Zhujun Yuan, Guang Bian, Tay-Rong Chang, Hao Zheng, Vladimir N. Strocov, Daniel S. Sanchez, Guoqing Chang, Chenglong Zhang, Daixiang Mou, Yun Wu, Lunan Huang, Chi-Cheng Lee, Shin-Ming Huang, BaoKai Wang, Arun Bansil, Horng-Tay Jeng, Titus Neupert, Adam Kaminski, Hsin Lin, Shuang Jia, and M. Zahid Hasan, "Discovery of a weyl fermion state with fermi arcs in niobium arsenide," Nat. Phys. **11**, 748–754 (2015).
[34] B. Q. Lv, N. Xu, H. M. Weng, J. Z. Ma, P. Richard, X. C. Huang, L. X. Zhao, G. F. Chen, C. E. Matt, F. Bisti, V. N. Strocov, J. Mesot, Z. Fang, X. Dai, T. Qian, M. Shi, and H. Ding, "Observation of Weyl nodes in TaAs," Nat. Phys. **11**, 724–727 (2015).
[35] L. X. Yang, Z. K. Liu, Y. Sun, H. Peng, H. F. Yang, T. Zhang, B. Zhou, Y. Zhang, Y. F. Guo, M. Rahn, D. Prabhakaran, Z. Hussain, S. K. Mo, C. Felser, B. Yan, and Y. L. Chen, "Weyl semimetal phase in the noncentrosymmetric compound taas," Nat. Phys. **11**, 728–732 (2015).
[36] Satya K. Kushwaha, Jason W. Krizan, Benjamin E. Feldman, Andrs Gyenis, Mallika T. Randeria, Jun Xiong, Su-Yang Xu, Nasser Alidoust, Ilya Belopolski, Tian Liang, M. Zahid Hasan, N. P. Ong, A. Yazdani, and R. J. Cava, "Bulk crystal growth and electronic characterization of the 3D Dirac semimetal Na_3Bi," APL Mat. **3**, 041504 (2015).
[37] Su-Yang Xu, Chang Liu, Satya K. Kushwaha, Raman Sankar, Jason W. Krizan, Ilya Belopolski, Madhab Neupane, Guang Bian, Nasser Alidoust, Tay-Rong Chang, Horng-Tay Jeng, Cheng-Yi Huang, Wei-Feng Tsai, Hsin Lin, Pavel P. Shibayev, Fang-Cheng Chou, Robert J. Cava, and M. Zahid Hasan, "Observation of fermi arc surface states in a topological metal," Science **347**, 294–298 (2015).
[38] Tian Liang, Quinn Gibson, Mazhar N. Ali, Minhao Liu, R. J. Cava, and N. P. Ong, "Ultrahigh mobility and giant magnetoresistance in the Dirac semimetal Cd3As2," Nat. Mater. **14**, 280–284 (2015).
[39] G. E. Volovik, *The Universe in a Helium Droplet* (Clarendon Press, 2003).
[40] A A Burkov and Leon Balents, "Weyl Semimetal in a Topological Insulator Multilayer," Phys. Rev. Lett. **107**, 127205 (2011).
[41] A A Zyuzin, Si Wu, and A A Burkov, "Weyl semimetal with broken time reversal and inversion symmetries," Phys. Rev. B **85**, 165110 (2012).
[42] Vivek Aji, "Adler-Bell-Jackiw anomaly in Weyl semimetals: Application to pyrochlore iridates," Phys. Rev. B **85**, 241101 (2012).
[43] Adolfo G Grushin, "Consequences of a condensed matter realization of Lorentz-violating QED in Weyl semimetals," Phys. Rev. D **86**, 045001 (2012).
[44] Chao-Xing Liu, Peng Ye, and Xiao-Liang Qi, "Chiral gauge field and axial anomaly in a Weyl semimetal," Phys. Rev. B **87**, 235306 (2013).
[45] Pallab Goswami and Sumanta Tewari, "Axionic field theory of (3+1)-dimensional Weyl semimetals," Phys. Rev. B **88**, 245107 (2013).
[46] Karl Landsteiner, "Anomalous transport of Weyl fermions in Weyl semimetals," Phys. Rev. B **89**, 075124 (2014).
[47] J. Klier, I. V. Gornyi, and A. D. Mirlin, "Transversal magnetoresistance in weyl semimetals," Phys. Rev. B **92**, 205113 (2015).
[48] Daniel Bulmash and Xiao-Liang Qi, "Quantum oscillations in weyl and dirac semimetal ultrathin films," Phys. Rev. B **93**, 081103 (2016).
[49] Y. Ominato and M. Koshino, "Magnetotransport in the Weyl semimetal in the quantum limit - the role of the topological surface states," ArXiv e-prints (2015), arXiv:1512.08223 [cond-mat.mes-hall].
[50] Mahito Kohmoto, Bertrand I. Halperin, and Yong-Shi Wu, "Diophantine equation for the three-dimensional quantum hall effect," Phys. Rev. B **45**, 13488–13493 (1992).
[51] Yasumasa Hasegawa, "Energy spectrum of electrons on three dimensional lattice in external magnetic field," Journal of the Physical Society of Japan **61**, 1657–1662 (1992), http://dx.doi.org/10.1143/JPSJ.61.1657.
[52] M. Koshino, H. Aoki, K. Kuroki, S. Kagoshima, and T. Osada, "Hofstadter butterfly and integer quantum hall effect in three dimensions," Phys. Rev. Lett. **86**, 1062–1065 (2001).
[53] M. Koshino, H. Aoki, T. Osada, K. Kuroki, and S. Kagoshima, "Phase diagram for the hofstadter butterfly and integer quantum hall effect in three dimensions," Phys. Rev. B **65**, 045310 (2002).
[54] Jun Goryo and Mahito Kohmoto, "Polarization of bloch electrons and berry phase in the presence of electromagnetic fields," Phys. Rev. B **66**, 085118 (2002).
[55] M. Koshino and H. Aoki, "Integer quantum hall effect in isotropic three-dimensional crystals," Phys. Rev. B **67**, 195336 (2003).
[56] Mikito Koshino and Hideo Aoki, "Integer quantum hall effect and hofstadter's butterfly spectra in three-dimensional metals in external periodic modulations," Phys. Rev. B **69**, 081303 (2004).
[57] J. Brüning, V. V. Demidov, and V. A. Geyler, "Hofstadter-type spectral diagrams for the bloch electron in three dimensions," Phys. Rev. B **69**, 033202 (2004).
[58] Tena Dubček, Colin J. Kennedy, Ling Lu, Wolfgang Ketterle, Marin Soljačić, and Hrvoje Buljan, "Weyl points

in three-dimensional optical lattices: Synthetic magnetic monopoles in momentum space," Phys. Rev. Lett. **114**, 225301 (2015).
[59] Dan-Wei Zhang, Shi-Liang Zhu, and Z. D. Wang, "Simulating and exploring weyl semimetal physics with cold atoms in a two-dimensional optical lattice," Phys. Rev. A **92**, 013632 (2015).
[60] W.-Y. He, S. Zhang, and K. T. Law, "The Realization and Dectection of Weyl Semimetals and Chiral Anomaly in Cold Atomic Systems," ArXiv e-prints (2015), arXiv:1501.02348 [cond-mat.quant-gas].
[61] Miguel A N Araújo and Eduardo V Castro, "Chern band insulators in a magnetic field," Journal of Physics: Condensed Matter **26**, 075501 (2014).
[62] By inspection of the spectrum it seems likely that given a commensurate value of $\Phi/\Phi_0 = p/q$ there is a particular value of k_z where q Weyl nodes appear somewhere in the spectrum (not necessarily at E=0). Unfortunately we have no rigorous proof and thus leave it as a conjecture (see supplementary information).
[63] X.G. Wen and A. Zee, "Winding number, family index theorem, and electron hopping in a magnetic field," Nuclear Physics B **316**, 641 – 662 (1989).
[64] L. Lepori, I. C. Fulga, A. Trombettoni, and M. Burrello, "Pt invariant weyl semimetals in gauge symmetric systems," ArXiv:1506.04761.
[65] More generally, the degeneracy will be some multiple nq of q for integer, since we know that if n Weyl pairs exist, then we can create nq copies by shifting k_y. For all the cases considered in this paper, $n = 1$.
[66] Alexandre Dauphin and Nathan Goldman, "Extracting the chern number from the dynamics of a fermi gas: Implementing a quantum hall bar for cold atoms," Phys. Rev. Lett. **111**, 135302 (2013).
[67] Z. Li, H.-Q. Wang, D.-W. Zhang, S.-L. Zhu, and D.-Y. Xing, "Dynamics of Weyl quasiparticles emerged in an optical lattice," ArXiv e-prints (2016), arXiv:1605.07280 [cond-mat.quant-gas].
[68] M. Aidelsburger, M. Lohse, C. Schweizer, M. Atala, J. T. Barreiro, S. Nascimbene, N. R. Cooper, I. Bloch, and N. Goldman, "Measuring the Chern number of Hofstadter bands with ultracold bosonic atoms," Nat. Phys. **11**, 162–166 (2015).
[69] Gregor Jotzu, Michael Messer, Remi Desbuquois, Martin Lebrat, Thomas Uehlinger, Daniel Greif, and Tilman Esslinger, "Experimental realization of the topological haldane model with ultracold fermions," Nature **515**, 237–240 (2014).
[70] Markus Greiner, Olaf Mandel, Tilman Esslinger, Theodor W Hänsch, and Immanuel Bloch, "Quantum phase transition from a superfluid to a mott insulator in a gas of ultracold atoms," Nature **415**, 39–44 (2002).
[71] Maxime Ben Dahan, Ekkehard Peik, Jakob Reichel, Yvan Castin, and Christophe Salomon, "Bloch oscillations of atoms in an optical potential," Phys. Rev. Lett. **76**, 4508–4511 (1996).
[72] Philipp T Ernst, Sören Götze, Jasper S Krauser, Karsten Pyka, Dirk-Sören Lühmann, Daniela Pfannkuche, and Klaus Sengstock, "Probing superfluids in optical lattices by momentum-resolved bragg spectroscopy," Nature Physics **6**, 56–61 (2010).
[73] A uniform population of the band is expected if the hierarchy of energy scales $\Delta \gg k_B T \gg W$ is satisfied, where W is the bandwidth Δ is the band gap and $k_B T$ is the temperature energy scale. This criterion is satisfied for high flatness ratios, which have been demonstrated in experiment [68].
[74] Di Xiao, Ming-Che Chang, and Qian Niu, "Berry phase effects on electronic properties," Rev. Mod. Phys. **82**, 1959–2007 (2010).
[75] See Supplemental Material at ??? for details on determining the Chern number profile from finite-k_z-width wavepackets and an argument supporting the possibility of emergent Weyl nodes at arbitrary flux.
[76] P Streda, "Theory of quantised hall conductivity in two dimensions," Journal of Physics C: Solid State Physics **15**, L717 (1982).
[77] Immanuel Bloch, Jean Dalibard, and Wilhelm Zwerger, "Many-body physics with ultracold gases," Rev. Mod. Phys. **80**, 885–964 (2008).
[78] Y.-Q. Wang and X.-J. Liu, "A Scaling Behavior of Bloch Oscillation in Weyl Semimetals," ArXiv e-prints (2016), arXiv:1605.02671 [cond-mat.mes-hall].
[79] Xiong-Jun Liu, K. T. Law, and T. K. Ng, "Realization of 2d spin-orbit interaction and exotic topological orders in cold atoms," Phys. Rev. Lett. **112**, 086401 (2014).
[80] Pallab Goswami and Sudip Chakravarty, "Quantum criticality between topological and band insulators in $3 + 1$ dimensions," Phys. Rev. Lett. **107**, 196803 (2011).
[81] Hiroki Isobe and Naoto Nagaosa, "Theory of a quantum critical phenomenon in a topological insulator: (3+1)-dimensional quantum electrodynamics in solids," Phys. Rev. B **86**, 165127 (2012).
[82] Gregory Gorohovsky, Rodrigo G. Pereira, and Eran Sela, "Chiral spin liquids in arrays of spin chains," Phys. Rev. B **91**, 245139 (2015).
[83] Chui-Zhen Chen, Juntao Song, Hua Jiang, Qing-feng Sun, Ziqiang Wang, and X. C. Xie, "Disorder and metal-insulator transitions in weyl semimetals," Phys. Rev. Lett. **115**, 246603 (2015).